Outer Membrane Monolayer Domains from Two-Dimensional Surface Scanning Resistance Measurements

Kenichi Suzuki, Ronald E. Sterba, and Michael P. Sheetz
Department of Cell Biology, Duke University Medical Center, Durham, North Carolina 27710 USA

ABSTRACT Cellular plasma membranes have domains that are defined, in most cases, by cytoskeletal elements. The outer half of the bilayer may also contain domains that organize glycosylphosphatidylinositol (GPI)-linked proteins. To define outer membrane barriers, we measured the resistive force on membrane bound beads as they were scanned across the plasma membrane of HEPA-OVA cells with optical laser tweezers. Beads were bound by antibodies to fluorescein-phosphatidylethanolamine (Fl-PE) or to the class I major histocompatibility complex (MHC class I) Qa-2 (a GPI-anchored protein). Two-dimensional scans of resistive force showed both occasional, resistive barriers and a velocity-dependent, continuous resistance. At the lowest antibody concentration, which gave specific binding, the continuous friction coefficient of Qa-2 was consistent with that observed by single-particle tracking (SPT) of small gold particles. At high antibody concentrations, the friction coefficient was significantly higher but decreased with increasing temperature, addition of deoxycholic acid, or treatment with heparinase I. Barriers to lateral movement ($>$3 times the continuous resistance) were consistently observed. Elastic barriers (with elastic constants from 1 to 20 pN/μm and sensitive to cytochalasin D) and small nonelastic barriers ($<$100 nm) were specifically observed with beads bound to the GPI-linked Qa-2. We suggest that GPI-linked proteins interact with transmembrane proteins when aggregated by antibody-coated beads and the transmembrane proteins encounter cytoplasmic barriers to lateral movement. The barriers to lateral movement are dynamic, discontinuous, and low in density.

INTRODUCTION

The cell plasma membrane is a heterogeneous structure that contains domains and patches (Sheetz, 1995; Kusumi and Sako, 1996; Edidin, 1997). It has been found that specialized membrane domains such as caveolae (Anderson, 1998), clathrin-coated pits (Kirchausen et al., 1997), and pre- and postsynaptic zones (Uchida et al., 1996) play crucial roles in several cell activities. Previously, membrane domains have been studied mainly with respect to the interactions between integral proteins and the underlying cytoskeletal proteins, such as the band 3-spectrin (Koppel et al., 1981; Kusumi and Sako, 1996) and E-cadherin-actin filament interactions (Kusumi et al. 1993; Sako and Kusumi, 1998). On the other hand, lipid microdomains have also been suggested to play a role. Simons and colleagues recently proposed that sphingolipid-cholesterol rafts form a platform for signal transduction and for protein and lipid transport from the trans-Golgi network to the plasma membrane (Simons and Ikonen, 1997).

Many studies of the lateral organization of cell membranes have been carried out by a variety of methodologies, such as atomic force microscopy (AFM) (Takeuchi et al., 1998), fluorescence recovery after photobleaching (FRAP) (Edidin and Stroynowski, 1991), near-field scanning optical microscopy (NSOM) (Endere et al., 1997; Hwang et al., 1998), single-particle tracking (SPT) (Sheets et al., 1997), and laser tweezers (Kucik et al., 1991; Edidin et al., 1991; Sako et al., 1995). SPT has enabled us to observe individual diffusing membrane proteins and revealed that there are distinct classes of protein diffusion, including simple Brownian motion, confined diffusion, and directed diffusion (Sheetz et al., 1989; Kusumi et al., 1993; Felsenfeld et al., 1996; Sheets et al., 1997). SPT studies have further indicated that plasma membranes in a variety of cells are compartmentalized into many small domains, in terms of lateral diffusion of membrane proteins (Tomishige et al., 1998; Sheets et al., 1997). This diffusive behavior of membrane proteins has also been investigated theoretically to show that the membrane protein diffusion is largely retarded by protein crowding effects (Saxton, 1990) and hydrodynamic effects of mobile or immobile proteins (Bussell et al., 1995a,b; Dodd et al., 1995).

The laser tweezers method has further allowed us to manipulate the cell to measure the force imposed on biological components in the range from 0.1 pN to 200 pN and to investigate mechanical properties in cell membranes. For example, Edidin et al. dragged 40-nm gold particles coated with antibodies to transmembrane MHC class I (H-2D^b) or glycosylphosphatidylinositol (GPI)-anchored MHC class I (Qa-2) molecules in HEPA-OVA cell membranes with laser tweezers (Edidin et al., 1991). They coined a new term, barrier free path length (BFP), to describe the distance between barriers that caused a bead to escape from the laser trap. BFP for the GPI-anchored protein Qa-2 was 8.5 μm at 34°C, which was much longer than for H-2D^b (3.5 μm), indicating the barriers to lateral movement are primarily on the cytoplasmic half of the membrane.

Although previous studies with optical laser tweezers have revealed barriers to the diffusion of membrane pro-

Received for publication 11 March 1999 and in final form 7 February 2000.

Address reprint requests to Michael P. Sheetz, Department of Biological Sciences, PO Box 2408, Columbia University, Sherman Fairchild Center, Rm. 713, 1212 Amsterdam Ave., New York, NY 10027. Tel.: 212-854-4857, lab 4-8133; Fax: 212-865-8246; E-mail: ms2001@columbia.edu.

0006-3495/00/07/448/12 $2.00

teins, the nature of the barriers could not be surveyed because the scan was limited to one dimension. Little is known about the relationship between barriers observed by laser tweezers experiments and the regions of confined diffusion observed by SPT. Furthermore, because previous studies of optical tweezers have been qualitative, it was difficult to identify the mechanism of inhibition of diffusion of membrane components, except by the membrane skeleton fence (Edidin et al., 1991: Sako and Kusumi, 1995), although extracellular matrix and/or lipid microdomains are also potential candidates. Therefore, systematic and quantitative analysis was needed to obtain a full understanding of the size, density, and characteristics of membrane barriers, which is essential for elucidating membrane structure and diffusion behavior. A method was developed here to map the barriers to lateral transport of outer leaflet components, GPI-anchored protein Qa-2, and fluorescein phosphatidylethanolamine (Fl-PE), by laterally dragging beads held in a laser trap attached to cell components in two dimensions. When the bead attached to antigen encounters membrane resistance during the scan, the bead is displaced from the trap center by a distance proportional to the viscous resistance force. We detected the displacement with a quadrant detector that provides high spatial and temporal resolution. Beads attached to a cross-linked GPI-anchored protein, Qa-2, encountered elastic, cytoplasmic barriers to lateral movement, but Fl-PE-attached beads did not. Moreover, the continuous resistance to lateral transport scaled with bead velocity, antibody density, and bead size. Resistance decreased with increasing temperature and heparinase and deoxycholate addition. The method described here provides novel information about the characteristics and density of barriers and viscous resistance to lateral transport of GPI-linked membrane proteins.

MATERIALS AND METHODS

Cell culture

HEPA-OVA mouse hepatoma cells that expressed an H-2D major histocompatibility complex (MHC) class I protein and were transfected with a Qa-2 gene were kindly provided by Dr. M. Edidin. HEPA-OVA cells were cultured in Dulbecco's modified Eagle's medium (DMEM) (Gibco Laboratories, Grand Island, NY) containing 10% fetal calf serum (Gibco Laboratories) and 300 μg/ml G-418 (Sigma, St. Louis, MO). To prepare the cell growth wells, 22 $\times$ 22 mm (no. 1½) glass coverslips (Corning, New York, NY) were cleaned by soaking in 20% nitric acid for 20 min, followed by rinsing in distilled water for 1 h. The cleaned coverslips were soaked in acetone for 2 min and silanized by dipping in 1,1,1,3,3,3-hexamethyldisilazane (Aldrich Chemical Co., Milwaukee, WI). After drying and sterilization, 22-mm-diameter cloning cylinders (Bellco, Vineland, NJ) were secured to the coverslips with sylgard (Dow Corning Corporation, Midland, MI). The growth well was coated with 0.01% poly-L-lysine for 15 min and rinsed three times with sterilized Dulbecco's phosphate-buffered saline buffer (Gibco Laboratories) and once with DMEM. Cells were seeded in cell growth wells (4×10^3/well) and grown for 18–30 h before the experiment was started.

Fluorescein Phosphatidylethanolamine Labeling of HEPA-OVA Cell Plasma Membranes

To label HEPA-OVA cells with fluorescein phosphatidylethanolamine (Fl-PE) (Molecular Probes, Eugene, OR), cells were incubated with 1 μg/ml of Fl-PE in serum-free DMEM for 10 min at 37°C, washed with fresh DMEM, and then examined in the microscope.

Treatment of cell membrane with enzyme or chemicals

HEPA-OVA cells in the growth well were washed with serum-free DMEM three times and treated with 5 U heparinase I from *Flavobacterium heparinum* (Sigma) in serum-free DMEM for 30 min at 37°C. After the heparinase I solution was removed, the cells were washed two times with serum-free DMEM and subsequently used for the scanning experiment in DMEM. In the case of treatment with cytochalasin D or sodium deoxycholate, cells were incubated with DMEM containing 1 μg/ml cytochalasin D or 0.2 mM sodium deoxycholate for 30 min at 37°C before the scanning experiment was performed in the same medium.

Bead preparation

Polystyrene latex beads that contain surface carboxyl groups (Polyscience, Warrington, PA) were activated with carbodiimide and then coated with bovine serum albumin (BSA) (Sigma). The BSA was then biotinylated with 60 μM NHS-LC-biotin (Pierce, Rockford, IL) and further incubated with avidin neutralite overnight at 4°C (Molecular Probes). The monoclonal antibody to Qa-2 was a gracious gift from Dr. Edidin, and the anti-fluorescein antibody was from Molecular Probes. Antibodies were incubated with NHS-LC-biotin for 2 h at room temperature and dialyzed against PBS overnight at 4°C. Then 20 μl of biotinylated antibody (10 μg/ml) was incubated with 15 μl of the bead solution (2.5 vol%) for 2 h at room temperature.

Microscope and laser tweezers manipulation

Before the sample was observed, the cloning cylinder was removed from the cell growth well, and the antibody-coated bead solution in the medium was put on the coverslip. Then the coverslip was mounted on a glass slide with silicon grease. The cell sample was mounted on a piezoelectric stage, which was fixed on top of a three-plate stage of a differential interference contrast (DIC) inverted microscope (Axiovert100S; Carl Zeiss, Oberkochen, Germany). The cell sample was illuminated by a 100-W halogen lamp using light of wavelength longer than 640 nm. The stage was maintained at 37°C with an air current incubator. The laser trap consisted of a beam from a 11-W TEM00 near-infrared Nd-YAG (wavelength 1064 nm) laser (model 116F; Quantronics Lasers, Hauppauge, NY). The laser output was expanded with a 4$\times$ beam expander (Newport, Irvine, CA) and spatially filtered to a 7-mm diameter beam. The resulting 1-W beam was further attenuated with a film polarizer and a Glan Thompson prism (Melles Griot, Irvine, CA). The laser was then focused through a 76-mm-focal length achromatic lens (Melles Griot) into the bottom port of the microscope and into a 100$\times$ PlanNeofluor objective lens. To attach the antibody-coated bead to the cell membrane, the bead was trapped at a trapping stiffness of 0.08 pN/nm and then lowered and held on the cell membrane for 4 s. The bright-field image of cell and bead was transmitted through the bottom port of the microscope and was reflected by a dichroic mirror to a partially silvered mirror. This partially silvered mirror reflected 90% of the light to the quadrant detector and passed the remaining 10% to the camera. To observe a DIC image with the camera, an analyzing polarizer was placed between the mirror and the camera. IR filters (model

E975SP; Chroma, Brattleboro, VT) were used to prevent the 1064-nm laser trap light from reaching the camera and quadrant detector.

Stiffness of the laser tweezers

The stiffness of the laser optical trap was estimated from the viscous drag in an aqueous medium in the microscope focal plane as previously reported (Dai and Sheetz, 1995) and by measuring the Brownian motion of a trapped bead (Simmons et al., 1996). The position of the bead in the trap was detected with a quadrant detector. In the case of the former method, the calibration displayed a very linear force-distance relationship for the optical tweezers down to a subpiconewton range. In the case of the latter method, the stiffness of laser tweezers, k, was calculated from the following equation by measuring the mean square Brownian motion of a bead along one axis, $\langle \Delta X^2 \rangle$: $\frac{1}{2}k\langle \Delta X^2 \rangle = \frac{1}{2}k_B T$, where k_B is Boltzmann's constant and T is the absolute temperature. The two estimations of laser stiffness were consistent with each other.

Quadrant detector and motion control of piezoelectric stage

Our quadrant detector system was able to detect and record the position of an immobile 1-μm bead with a spatial resolution of 1 nm at a sampling rate of several kilohertz. The quadrant detector was a set of four silicon photodiodes. The photosensitive areas of all four diodes were arranged as different quadrants forming a circular detector 1 mm in diameter (Hamamatsu 1557). The current flowing through the photodiode element was linearly proportional to the intensity of light projected onto each of the quadrants. The bright-field image of a bead held in the laser trap was focused and magnified so that it was about half the diameter of the quadrant detector and centered on the detector face. To convert horizontal and vertical displacements of the bead to corresponding voltage signals, a four-stage electronic circuit was built (Simmons et al., 1996).

In the first stage of the circuit, the current flowing through each photodiode was converted to a proportional voltage by low-noise transimpedance amplifiers. To convert these individual quadrant signals to horizontal and vertical displacement signals, the second and third stages of the circuit performed steps of analog addition and subtraction on the quadrant voltage signals. A vertical signal resulted from the sum of the two upper quadrants subtracted from the sum of the two lower quadrants. Similarly, the sum of the two left quadrants subtracted from the sum of the two right quadrants results in a horizontal signal. The fourth stage of the circuit was a second-order Butterworth filter with a cutoff of 1.2 kHz.

To detect and record the position signal, a 12-bit A-to-D computer digitizer was used. The computer was programmed to display a trace of the vertical and horizontal position of the bead while the data were being collected. To scan the bead across the cell surface, a D-to-A computer board was used to send voltage signals to control the position of the piezoelectric stage via a high-voltage amplifier (Wye Creek Instruments, Fredricksburg, MD).

Detection of the *z* position of the bead

When the z position of a bead changes, the white area of the DIC image of the bead also changes. Therefore, by measuring the white area of the bead we can detect the z position of a bead near the focal plane. The white area was measured every 50 nm with National Institutes of Health Image. We then calculated the relationship between the white area and the z position of the bead that was set by a piezo controller (Physik Instrumente, Waldbronn, Germany). Relative position changes of ± 20 nm were detected reliably.

Observation by scanning electron microscopy

Cells were rinsed with Hanks' balanced salt solution (HBSS) (Gibco Laboratories, Grand Island, NY) three times, fixed with 2.5% glutaraldehyde in 0.1 M cacodylate buffer (pH 7.4) for 15 min, and postfixed with 1% OsO_4 in distilled water for 30 min at 4°C. After dehydration through a graded series of ethanol solutions, the cells were immersed in tetramethylsilane (TMS) ($Si(CH_3)_4$; Electron Microscopy Sciences, Fort Washington, PA) for 10 min and air-dried at room temperature. All specimens were mounted on aluminum stubs with carbon conducting tape and then sputter coated with a thin layer (~20 nm) of gold palladium, using a Hummel V Sputter coater (Anatech, Alexander, VA). Specimens were stored under vacuum until they were examined and imaged in a Philips 501 scanning electron microscope (Mahwah, NJ) at 15 kV.

RESULTS AND DISCUSSION

Specificity of bead binding to the cell membrane surface

To determine whether the antibody-coated beads bound specifically to the antigen, the probability of the bead binding was examined. Antibody-coated, 0.73-μm beads were held by laser tweezers (stiffness 0.08 pN/nm) on the cell membrane for 4 s, and then the laser was turned off. The binding probability of fluorescein or Qa-2 antibody-coated beads (0.73 μm) at 37°C was 59% ($n = 70$) and 55% ($n = 70$), respectively. If the cell was not labeled with Fl-PE, the binding probability of the anti-fluorescein antibody-coated bead was 11% ($n = 70$). Meanwhile, the probability of binding of the beads without antibody was also 11% ($n = 70$). Therefore, the antibody-coated beads were specifically bound to the cell surface antigen.

We also examined the percentage of attached beads that could be scanned in two dimensions. The mobile fraction of the attached beads was defined as the percentage of bound beads that could be dragged more than 2.9 μm (single scan length of the piezoelectric stage) with a tweezers force of ~10 pN. The mobile fractions were much greater for the lipid-linked beads, 78% for Fl-PE ($n = 42$), and 61% for Qa-2 ($n = 39$), than for transmembrane protein H-2D^b, which only had 10% mobile beads. The short barrier free path length of H-2D^b was consistent with the results described previously (Edidin et al., 1991) and did not allow 2-D scanning experiments. Lipid-linked beads were scanned in two dimensions over the cell lamella.

The concentration of the antibody incubated with 0.73-μm beads was 10 μg/ml at most. At higher antibody concentrations, the beads were frequently immobilized on the cell membrane. The trapping stiffness of the laser employed in these experiments was 0.08 pN/nm (maximum force of ~10 pN). At higher power levels, nonspecific binding of the bead to the cell membrane was enhanced, but at lower power levels, the bead frequently escaped from the laser trap during scanning.

2-D surface scanning and resistance mapping

To ensure that the piezoelectric stage tracked accurately, the track of a bead attached to a coverslip was examined during a two-dimensional scan by tracking the bead at 37°C (Gelles et al., 1988). As shown in Fig. 1 *A*, each scan line was straight and was separated by an equal distance from the next scan line. After the scan, the bead returned to the starting point (position change <30 nm). The *z* position of the bead changed less than ±50 nm, as determined by quantitative image analysis. Hysteresis was not observed in two subsequent scans. We note that there were occasional lateral displacements of the stage that were larger than the errors in the tracking measurement (standard deviation of the stuck bead position measurement was ~10 nm). We believe that those were due to mechanical inhomogeneities in the piezo stage, but their frequency and extent were so small that they did not affect these measurements (the location and frequency of the dislocations were random). The speed of the stage was steady, as shown in Fig. 1 *B*.

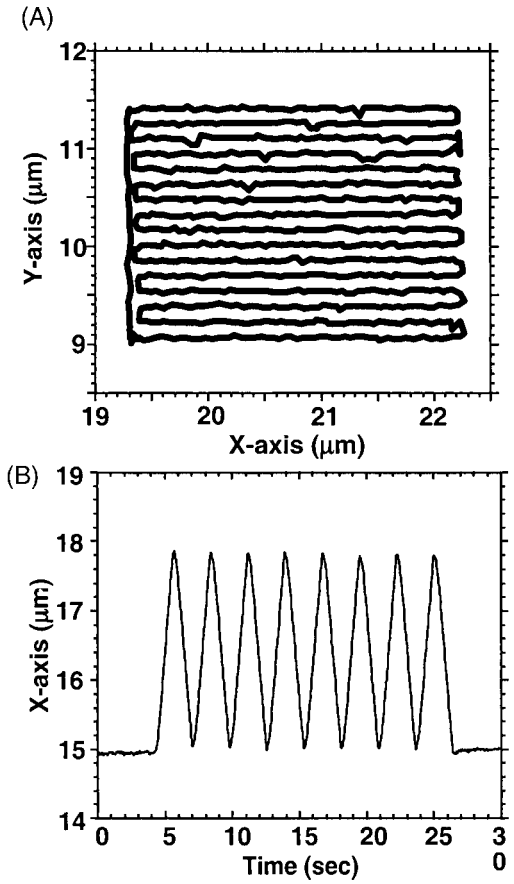

FIGURE 1 (*A*) Example of the scanning track of a 0.73-μm bead attached to the coverslip. (*B*) Example of the relationship between time and the piezostage movement. The piezoelectric stage position was regulated by a computer, using a 2-D scanning program. Bead position was determined by the single-particle tracking (SPT) method (Gelles et al., 1988).

These results show that motion control of the piezoelectric stage by the computer was conducted with sufficient accuracy for the experiment.

To examine the pattern of membrane resistance, beads were scanned over the same membrane region several times. In four different scans of one region over 2 min (Fig. 2), the regions of larger force were often seen in the next scan. The pattern of resistance to movement changed significantly from first to last scan, but some features were constant. It should be noted that the vertical analysis of the bead position showed no significant change in *z* position over these scans. There was a constant force on the bead due to the viscous resistance of the membrane outside of the high-resistance areas. The system is capable of measuring reproducible resistance features of the membrane, but the membrane is dynamic on the scale of minutes.

Measurement of the friction coefficient between the bead and the cell membrane

As shown in Fig. 3, the bead was displaced by a constant distance from the center of laser trap, which reflects the resistance of the viscous membrane medium. We defined the force on the bead that was not encountering a barrier as D_{resting}. D_{resting} did not significantly change, even if we changed *z* position of the bead by +50 nm or −50 nm before the scan. Another important parameter is the noise in the position measurements; $(X_{\text{average}} - X_{\text{i}})^2_{\text{average}}$ was defined as $\langle \Delta X^2 \rangle$ to evaluate a noise level (X_{average}, average value of distance from the trapping center; X_{i}, distance from the trapping center at the individual sampling point). If this displacement was caused by viscous drag of the cell membrane, the scale of displacement should change when the scan speed was changed. Fig. 4 *A* shows the relationship between the stage speed and D_{resting} when Qa-2 (GPI anchored protein) antibody-coated beads were laterally dragged at 37°C. The linear dependence of force on velocity was consistent with a Newtonian fluid. Using the equation $F = fv$, where F is force, f is a friction coefficient, and v is the velocity of bead movement, the friction coefficient between the Qa-2 beads and the cell membrane was estimated to be 1.31 ± 0.17 (pN/(μm/s)). As shown in Fig. 4 *B*, $\langle \Delta X^2 \rangle$ was not dependent on the scan speed and was at the same level as Brownian motion ($\langle \Delta X^2 \rangle$ = 47.6 ± 2.7 nm^2). Thus the noise level did not change with velocity and did not systematically affect the estimation of the friction coefficient.

If the bead was bound to the cell membrane nonspecifically, the friction coefficient was much smaller (estimated to be 0.18 ± 0.17 (pN/(μm/s)) than the friction coefficient observed with the Qa-2 antibody beads (1.31 ± 0.17 pN/(μm/s)). Although the probability of nonspecific bead binding (11%) was one-fifth of the probability of specific binding (55%), there were no Qa-2 antibody beads that had the friction coefficient of nonspecifically attached beads. Re-

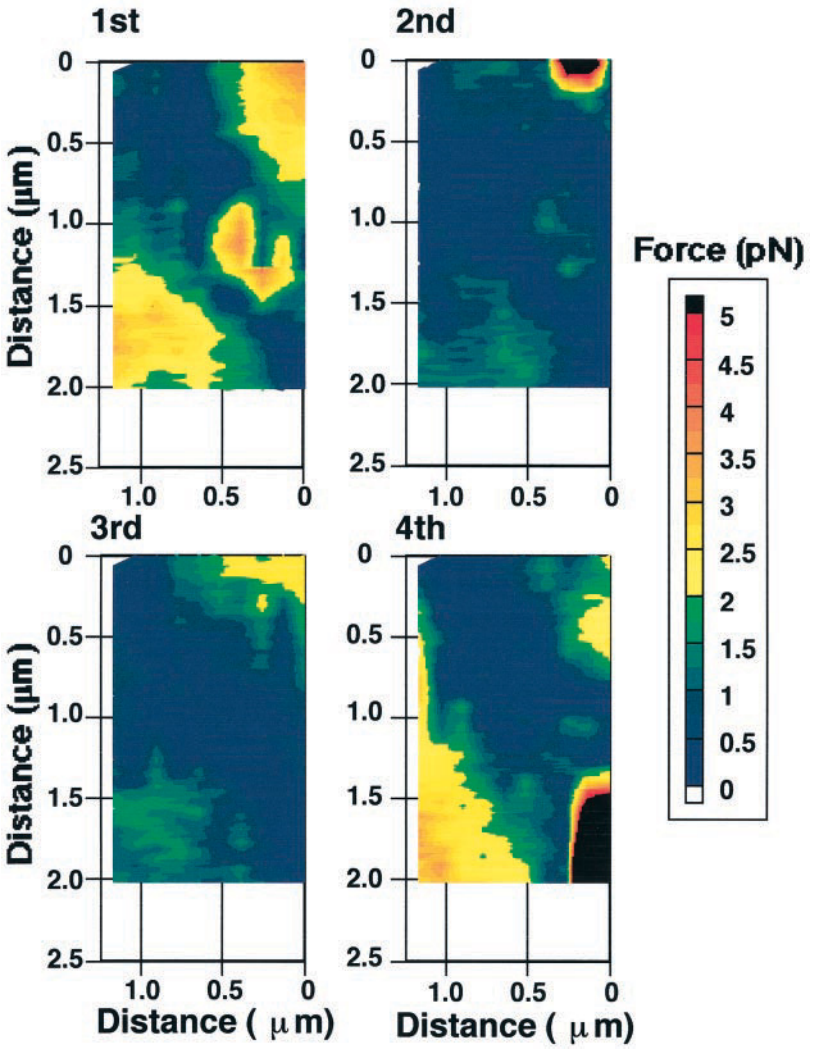

FIGURE 2 Two-dimensional scanning resistance of a laser-trapped bead coated with Qa-2 antibody on a HEPA-OVA cell membrane. The scan was performed 10 times (five times forward and five times backward, with scans separated by 130 nm laterally), using a Qa-2 antibody-coated bead at 1.0 μm/s. It took over 2 min to scan the same region four times. The bead position was detected with the quadrant detector at a sampling frequency of 300 points/μm.

cruitment of antigen could occur after a nonspecific binding event. The component of the total friction coefficient (1.31 pN/(μm/s)) of Qa-2 bound beads that is due to binding of antigen can be obtained by subtracting out the friction coefficient of nonspecifically bound beads (in this case 0.18 $\pm$ 0.04 pN/(μm/s)). In the analysis of the friction coefficient of the nonspecifically bound beads, 0.05 pN/(μm/s) is contributed by water, leaving only 0.13 pN/(μm/s) as the friction coefficient of the membrane surface. The Qa-2 antigen that was pulled through the membrane by the Qa-2 beads provided the majority of the resistance (the specific contribution to the friction coefficient was 1.13 pN/(μm/s) or 86% of the total value).

To evaluate the reliability of the friction coefficient measured by this methodology, we altered a variety of conditions that were known to affect the friction coefficient. When the temperature was decreased to 28 and 19°C, the friction coefficient was increased to 1.44 $\pm$ 0.17 (pN/(μm/s)) and 2.61 $\pm$ 0.47 (pN/(μm/s)), respectively (Table 1), whereas nonspecifically bound bead frictional coefficients increased only slightly with decreasing temperature. As predicted, decreasing temperature increased the friction. Incorporation of surfactants into the cell membrane is known to weaken the interaction between lipids. The friction coefficient of the anti Qa-2 beads with sodium deoxycholate (0.2 mM) was decreased to 0.81 $\pm$ 0.17 (pN/(μm/s)) (Table 1). In this case, the nonspecific contribution to the friction coefficient of the control Qa-2 antibody beads (0.13 pN/(μm/s)) is a small fraction of the change in friction coefficient with deoxycholate (0.5 pN/(μm/s)). The increase in the friction coefficient at the lower temperature is consistent with the decrease in the diffusion coefficient of Qa-2 measured by FRAP (Edidin et al., 1991). Moreover, the decrease in the friction coefficient with deoxycholate treatment (Table 1) is also in line with the increase in cell membrane fluidity measured by the fluorescence depolarization method (Schroder et al., 1996; Zhao and Hirst, 1990), which measures the membrane resistance to the rotational motion of fluorescence probes and provides a membrane microviscosity. The magnitude of change of the

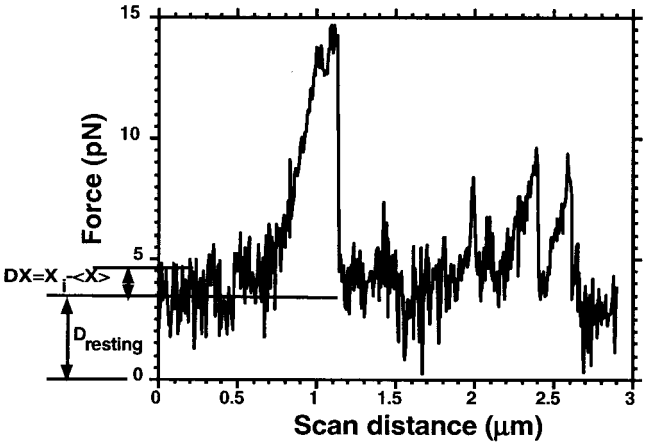

FIGURE 3 Definition of $D_{resting}$ and $\langle \Delta X^2 \rangle$. The scan was performed using a Qa-2 antibody-coated bead at 2.9 μm/s, 37°C. In this figure, the data were not averaged by the filter. Continuous displacement of bead from the trapping center was defined as $D_{resting}$. On the other hand, $(X_{average} - X_i)^2{}_{average}$ was defined as $\langle \Delta X^2 \rangle$ to evaluate a noise level. $X_{average}$, average value of distance from the trapping center; X_i, distance from the trapping center at the individual sampling point.

friction coefficient estimated from resistance correlates well with the relative changes in the friction coefficient measured by the membrane microviscosity.

To investigate the dependence of the friction coefficient on cell membrane components, fluorescein antibody beads bound to Fl-PE were examined (Table 1). The friction coefficient measured was 0.67 ± 0.07 (pN/(μm/s)), which was smaller than for the GPI-anchored protein Qa-2 (1.31 (pN/(μm/s)). To investigate the contribution from the pericellular matrix, we removed portions of carbohydrates by treating the cell with heparinase I (Table 1). The bead friction coefficient with the antibody to GPI-anchored protein Qa-2 dropped from 1.31 ± 0.17 (pN/(μm/s)) to 0.87 ± 0.20 (pN/(μm/s)); meanwhile that with the antibody to fluorescein decreased from 0.67 ± 0.07 (pN/(μm/s)) to 0.34 ± 0.07 (pN/(μm/s)). The decrease in the friction coefficient caused by the removal of extracellular carbohydrates is consistent with previously reported diffusion measurements (Lee et al., 1993), suggesting that the extracellular carbohydrates generate much of the resistance to diffusion of the membrane components.

The friction coefficient with the antibody to the GPI-anchored protein was approximately twofold larger than fluorescein. Because the binding probability of the Qa-2 bead was similar to that of the fluorescein bead, the number of binding sites may be similar. The greater friction coefficient appears to be due to differences in the friction coefficient of the bound components in the membrane. When the extracellular carbohydrates were removed by heparinase, the coefficient measured with the GPI-anchored protein was still larger than with Fl-PE; therefore, we suggest that the difference comes from the lipid bilayer and/or

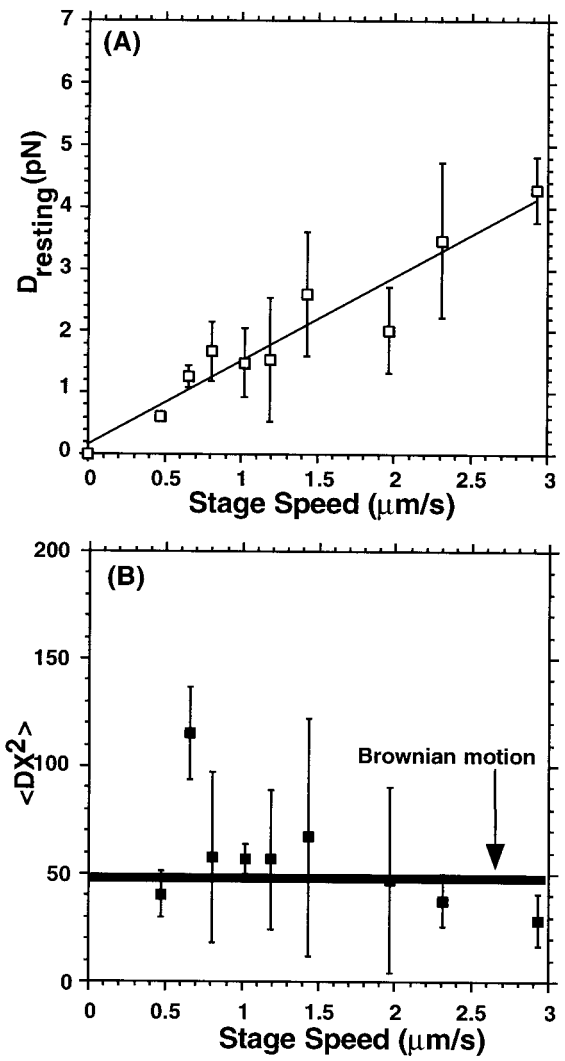

FIGURE 4 Plot of $D_{resting}$ (*A*) and $\langle DX^2 \rangle$ (*B*) against piezoelectric stage speed. Scanning was performed using a 0.73-μm Qa-2 antibody-coated bead at 37°C. For each scan speed, eight beads were analyzed (error bars represent standard error of the mean.

cytoskeletal layer. On the other hand, the magnitude of the change in resistivity caused by heparinase treatment was the same for Fl-PE and for Qa-2. Therefore, we suggest that the contribution of the friction between Qa-2 and extracellular carbohydrates is small and that the bead encounters the extracellular carbohydrates independently of the anchor because the bead is held close to the cell surface.

The friction coefficient of Qa-2 beads (0.73 μm) corresponds to a diffusion coefficient of (3.2 ± 0.4) × 10^{-11} cm^2/s (from the equation $D = kT/f$, where D is the diffusion coefficient, k is the Boltzmann constant, T is the absolute temperature, and f is the friction coefficient). This is comparable to the diffusion coefficient measured by SPT (5.5 ± 1.7) × 10^{-11} cm^2/s ($n = 5$) with a bead of the same size (0.73 μm), indicating that the surface scanning resistance (SSR) measurement is in good agreement with SPT measurements.

TABLE 1 Friction coefficient calculated from a linear least-squares fit of the plot of $D_{resting}$ against the dragging speed of antibody-bound bead

	Bead size (μm)	Temperature (°C)	Cell condition	Friction coefficient (pN/(μm/s))	Diffusion coefficient ($\times 10^{11}$ (cm^2/s)*
Qa-2	0.73	37.0	Nontreated	1.31 ± 0.17	3.26 ± 0.42
Qa-2	0.91	37.0	Nontreated	1.80 ± 0.36	2.37 ± 0.48
Qa-2	1.89	37.0	Nontreated	2.86 ± 1.01	1.49 ± 0.52
Qa-2	0.73	28.0	Nontreated	1.44 ± 0.17	2.97 ± 0.35
Qa-2	0.73	19.0	Nontreated	2.61 ± 0.47	1.64 ± 0.29
Qa-2	0.73	37.0	Heparinase treated	0.87 ± 0.20	4.91 ± 1.13
Qa-2	0.73	37.0	Deoxycholate treated	0.81 ± 0.17	5.27 ± 1.11
Fl-PE	0.73	37.0	Nontreated	0.67 ± 0.07	6.37 ± 0.67
Fl-PE	0.73	37.0	Heparinase treated	0.34 ± 0.07	12.56 ± 2.59

*The diffusion coefficient was estimated from the friction coefficient.

The diffusion coefficient estimated above was much smaller than the value observed by the SPT method with 40-nm gold particles, $(2.1 \pm 0.3) \times 10^{-10}$ cm^2/s (Edidin et al., 1991). In the case of the resistance to lipid movement, Sheets et al. developed a method for categorizing the lateral mobility of membrane components by classifying SPT trajectories into one of four modes of lateral transport: fast diffusion, slow diffusion, confined diffusion, and a stationary fraction (Sheets et al., 1997). The friction coefficient of Fl-PE, which we estimated here, corresponds to a diffusion constant of $(6.3 \pm 0.7) \times 10^{-11}$ cm^2/s. This is also smaller than the diffusion coefficient of the fast component that they measured with 40-nm gold particles, $(5.6 \pm 0.6) \times 10^{-10}$ cm^2/s, but similar to that of the slow one, $(3.8 \pm 0.6) \times 10^{-11}$ cm^2/s, and the confined one, $(5.5 \pm 1.6) \times 10^{-11}$ cm^2/s (Sheets et al., 1997). Therefore, the diffusion coefficient estimated from the friction coefficient with the 0.73-μm bead in our system is smaller than the diffusion coefficient of 40-nm gold particles measured by SPT. Differences in the diffusion coefficients could be related to the number of linkages between antibody and antigen, because the larger contact area is much more likely to involve additional membrane components at the bead-membrane interface.

Because the ratio of the antibody to the bead is 1000:1, the bead is most likely to be attached to the cell membrane via multivalent linkages, which would induce the aggregation of the linked cell membrane components within the contact area. To examine the dependence of membrane resistivity on the number of linkages, Qa-2 antibody concentration was diluted to one-tenth by mixing it with a nonbinding anti-fluorescein antibody (fluorescein/Qa-2 = 9:1, when Fl-PE was not incorporated into the cell membrane). The probability of binding of the 0.73-μm bead to the cell membrane was 26%, and the measured friction coefficient was 0.17 ± 0.02 (pN/(μm/s)) at 37°C, which is one-eighth of the coefficient found with the higher antibody concentration (1.31 ± 0.17 (pN/(μm/s), binding probability 55%). The nonspecific binding probability was 18%, and the friction coefficient of the beads, which were nonspecifically bound to the membrane, was 0.18 ± 0.04 (pN/(μm/s)), which is the same as that with the bead coated with diluted antibody concentration. Because the binding probability of beads linearly increased at the low specific antibody concentration as the concentration increased (Fig. 5), the binding probability of the diluted antibody bead is different from that of nonspecific antibody bead. Therefore, the same friction coefficient in the two cases indicates that the friction forces acting on the unknown nonspecific binding sites are similar to those acting on Qa-2. This friction coefficient corresponds to a diffusion constant of $(2.5 \pm 0.3) \times 10^{-10}$ cm^2/s for a single membrane protein, which is similar to the experimental value mentioned above, $(2.1 \pm 0.3) \times 10^{-10}$ cm^2/s (Edidin et al., 1991).

The friction coefficient of the beads with a high concentration of anti Qa-2 antibody was nearly 10-fold higher than

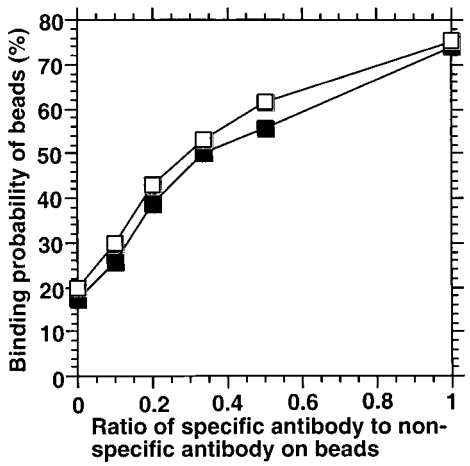

FIGURE 5 The binding probability of a Qa-2 antibody bead (0.73 μm) as a function of antibody density. The ratio of specific antibody (■, Qa-2 antibody; □, fluorescein antibody) to nonbinding antibody was changed from 0 to 1, keeping the total antibody concentration constant. The bead was trapped by laser tweezers, placed on the cell membrane, and held for 10 s.

with a low antibody concentration. Earlier observations indicated that the cross-linking of many transmembrane glycoproteins does not result in a significant increase in membrane resistance to diffusion (Kucik et al., 1999). To explain the dependence of the friction coefficient on antibody concentration, there are two likely explanations. In the first, the cross-linking of Qa-2s by the bead could result in recruitment of a transmembrane protein, which would have a significantly greater friction coefficient than Qa-2 itself. There is considerable evidence that GPI-anchored proteins associate with transmembrane and cytoplasmic proteins. For example, GPI-anchored proteins such as CD 59, Thy-1, and DAF were coprecipitated with a protein tyrosine kinase that is a cytoplasmic regulator of signal transduction (Stefanova et al., 1991; Shenoy-Scaria et al., 1992). Qa-2 is also believed to associate with cytoplasmic proteins, because Qa-2 mediates signaling to the cytoplasm (Hahn et al., 1992). Cytoplasmic protein interactions should increase membrane resistance for the GPI-anchored protein and we will show that Qa-2 antibody beads do interact with cytoplasmic barriers more than Fl-PE bound beads (below).

Another possibility is that the nearly 10-fold increase of the friction coefficient is due to a 10-fold higher number of the linkages between the bead and the cell membrane. The difference between the Con A beads, which Kucik et al. used (Kucik et al. 1999), and the Qa-2 antibody beads could be the difference in the permeability of lipid molecules into the bead-membrane contact area. If lipids can exchange freely into the contact area, the membrane is equally resistive to each Qa-2 molecule; therefore, the friction between the bead and the membrane should be proportional to the number of linkages. Because Con A-coated beads bind to membrane proteins nonspecifically, the density of transmembrane domains should be greater than with GPI-anchored proteins, which may prevent the free exchange of lipid into the contact region. If the friction coefficient is proportional to the number of linkages between the bead and membrane as in the free-draining regime (Kucik et al., 1999), the friction coefficient should increase in proportion to the contact area for larger beads, which had the same antibody density. Table 1 shows that the friction coefficient increased with increasing bead size. To estimate how the contact area changed with increasing bead size, the beads placed on the cell membrane surface with laser tweezers were observed by scanning electron microscopy (Fig. 6). The diameter of the contact area was found to be 220 $\pm$ 27 nm ($n = 8$) for the 0.73-μm beads, 240 $\pm$ 17 nm ($n = 8$) for the 0.91-μm beads, and 350 $\pm$ 44 nm ($n = 8$) for the 1.89-μm beads. The contact diameter can also be calculated by assuming that the fully extended length of the complex of BSA, biotin, avidin, and antibody is 25 nm (in other words, the surface of the bead can be linked to the membrane even when the bead surface is 25 nm above membrane) and the minimum length is 10 nm. With these estimates, the contact diameters are calculated to be 207 nm

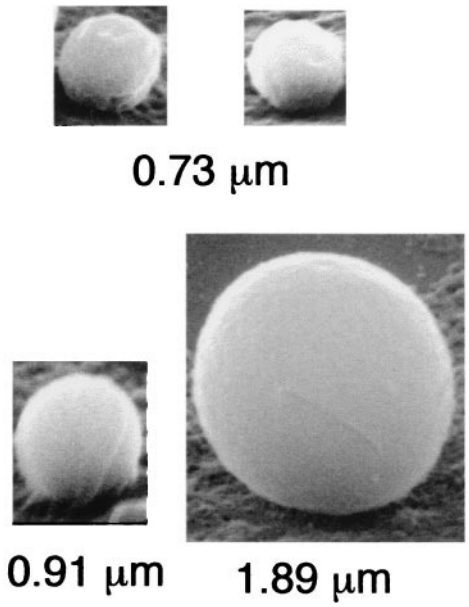

FIGURE 6 Scanning electron micrographs of antibody-coated 0.73-μm, 0.91-μm, and 1.89-μm beads on HEPA-OVA cell plasma membrane surfaces. Beads were trapped by laser tweezers, held on the membrane, and subsequently fixed with glutaraldehyde and osmium tetraoxide.

(0.73 μm bead), 230 nm (0.91 μm bead), and 336 nm (1.89 μm bead); the area of contact is 0.04 μm^2 (0.73 μm bead), 0.05 μm^2 (0.91 μm bead), and 0.10 μm^2 (1.89 μm bead), respectively. This result (Table 1 and Fig. 6) shows that the friction coefficient is proportional to the number of the major sources of the friction, which is consistent with a free-draining contact region.

Because the tweezers exert not only a force parallel with the cell membrane but also a torque lifting membrane components bound to the bead, there is a possibility that the cell membrane components are extracted by the torque (Evans et al., 1991). At the lowest antibody concentration on the bead surface, we found that the beads could be pulled off the surface with a force of 25 pN (41%) at the edge of the cell (the pulling rate was less than 0.5 μm/s). The ratio of the lateral force to the lifting force was calculated from the radius of the area of contact of the bead with the surface and the bead radius (see Appendix). A mechanical advantage of three- to fourfold for the 0.73-μm beads means that a steady force of 3–4 pN parallel to the surface is insufficient to pull components from the membrane. When some barriers are encountered, the parallel forces can reach 10 pN, which would be sufficient to pull some components from the membrane. With 0.73-μm beads, the resistance patterns are highly reproducible, and there is no indication that components are being pulled from the membrane. With larger 2.0-μm beads, the beads rolled at velocities higher than 2 μm/s, which suggests that components are being pulled from the membrane. It should be noted that the vertical force pulling bound components out of the membrane at the

trailing edge of the bead contact is balanced by a vertical force pushing the bead into the membrane at the leading edge of the contact. The pushing force could generate resistance to the bead movement from the carbohydrates. Under the conditions used in these studies, however, we do not believe that the components bound to the 0.73-μm beads are being pulled from the membrane.

Characterization of barriers to lateral movement

When the bead was dragged on the cell surface, two types of barriers were observed (Fig. 7 *A*). One has the elastic feature of recoil (*left*), and the other does not show recoil (*right*). We were often able to observe the same elastic displacement in repeated one-dimensional scans, although

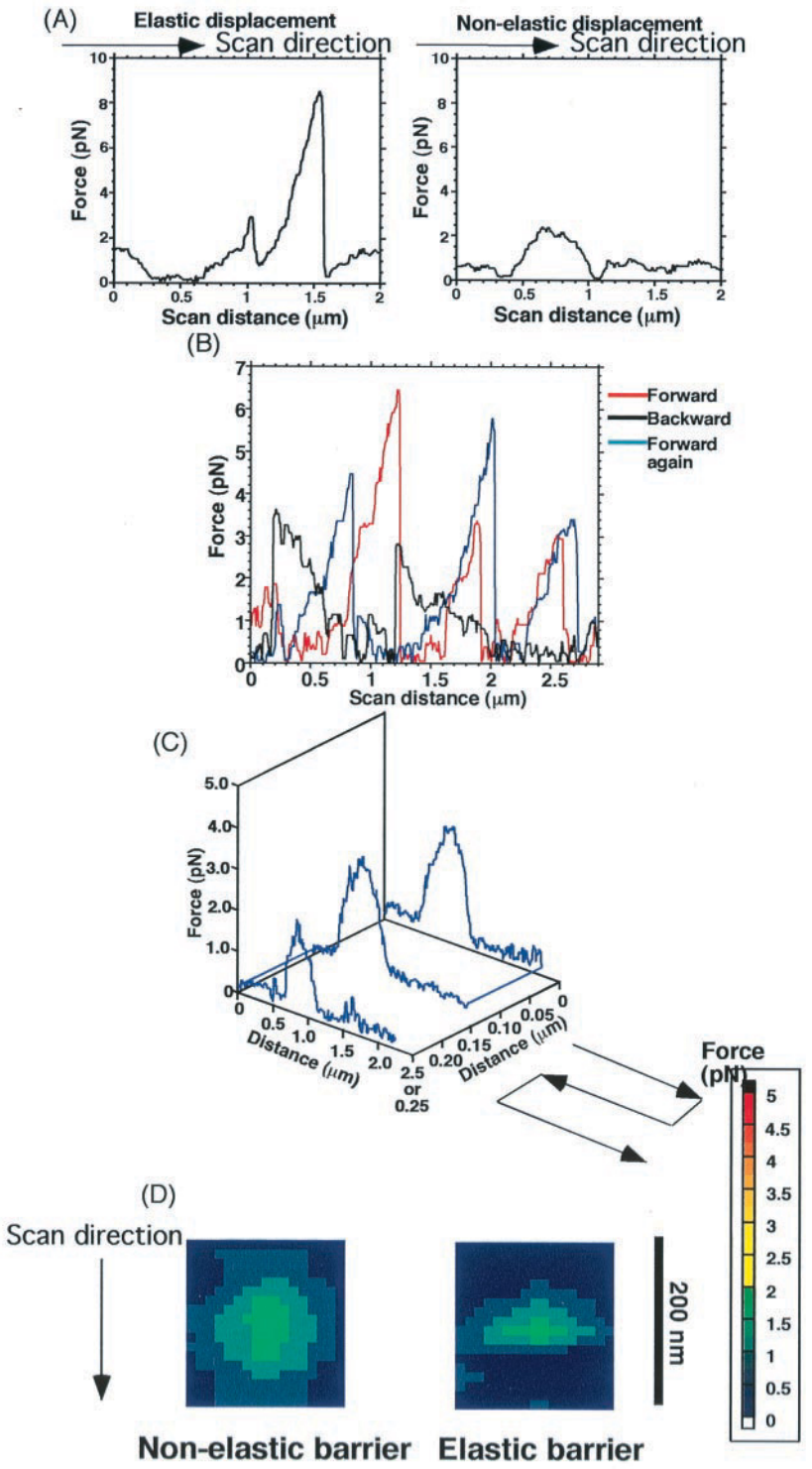

FIGURE 7 Profile of membrane barriers. All scans were performed at 1.0 μm/s. (*A*) Two types of barrier observed during the scan. The position of the 0.73-μm bead coated with Qa-2 antibody was detected with a quadrant detector at a sampling frequency of 300 points/μm. The data were filtered using a seven-point median filter. (*B*) Reproducibility of barrier displacements of a bead coated with Qa-2 antibody. The piezoelectric stage was moved forward, backward, and forward in one dimension. (*C*) Appearance of barriers in adjacent scans of a bead coated with Qa-2 antibody. (*D*) Types of barrier observed during the scan. Even if the size of the barriers was small, these were distinguishable.

the position and the strength of the barrier often changed slightly (Fig. 7 *B*). In two-dimensional scans, these barriers were often observed in the adjacent scan lanes, and the elastic stretch occurred in the opposite direction (Fig. 7 *C*). This indicates that some of the barriers are linear and extend in the direction perpendicular to a scan lane. Thus we can estimate the scale of a membrane barrier from the two-dimensional scan. Furthermore, even if the barrier size is small, we can distinguish between elastic barriers and nonelastic ones (Fig. 7 *D*). These results indicate that the quantitative measurement of the position of the bead, which is scanned over the cell plasma membrane in two dimensions, allows us to observe the size, density, and stiffness of two different types of membrane barriers. Previous studies, using one-dimensional scans, noted the location where a bead was drawn from the trap (Edidin et al., 1991) or used rebound (escape) of the latex bead tagged with transferrin to identify corral walls (Sako and Kusumi, 1995). We have extended that methodology to two dimensions with higher maximum force to observe not only the two-dimensional nature of corral walls, but also their elastic characteristics.

We wished to understand the basis and characteristics of the elastic barriers. Because the barriers are likely to be linked to the cell cytoskeleton, we treated cells with 1 μg/ml cytochalasin D, which resulted in the loss of two-thirds of the elastic barriers. The number of nonelastic barriers was not significantly altered by cytochalasin D, which indicates that the nonelastic barriers are not actin dependent. Because nonspecifically bound beads rarely showed recoil, the elastic barriers are not due to nonspecific binding of beads. Furthermore, elastic barriers were at control (nonspecific bound bead) levels for fluorescein-PE attached beads and for beads bound by a low concentration of antibody to Qa-2. The elastic constant of the barriers was in the range of 1–20 pN/μm, with a median value of 8.5 pN/μm. This is larger than for the transferrin receptor (3.0 pN/μm) (Sako and Kusumi, 1995) and for E-cadherin (3.5 pN/μm) (Sako and Kusumi, 1998). Because we employed a 0.73-μm bead, which is much larger than that of Sako et al. (0.21 μm), the number of membrane proteins linked to the bead in our system could be larger. As mentioned above, it is likely that the cross-linked GPI-anchored proteins bind a membrane-spanning protein, which interacts with the cytoskeletal proteins.

To quantify the nonelastic barriers, the barriers were categorized as a function of the area (the length in the scan direction times the width measured from subsequent scans) (Fig. 8). Fig. 8 *A* indicates that the size ranged from 50 nm to 1.5 μm in the scan direction (defined as d_s) and from a single lane to 10 consecutive lanes in the perpendicular direction (defined as d_p). Among these barriers, the smallest barrier (50 nm $< d_s <$ 100 nm in the scan direction and a single lane in the perpendicular direction) was most frequently observed with Qa-2 antibody beads. To determine whether cell membrane morphology (roughness) creates

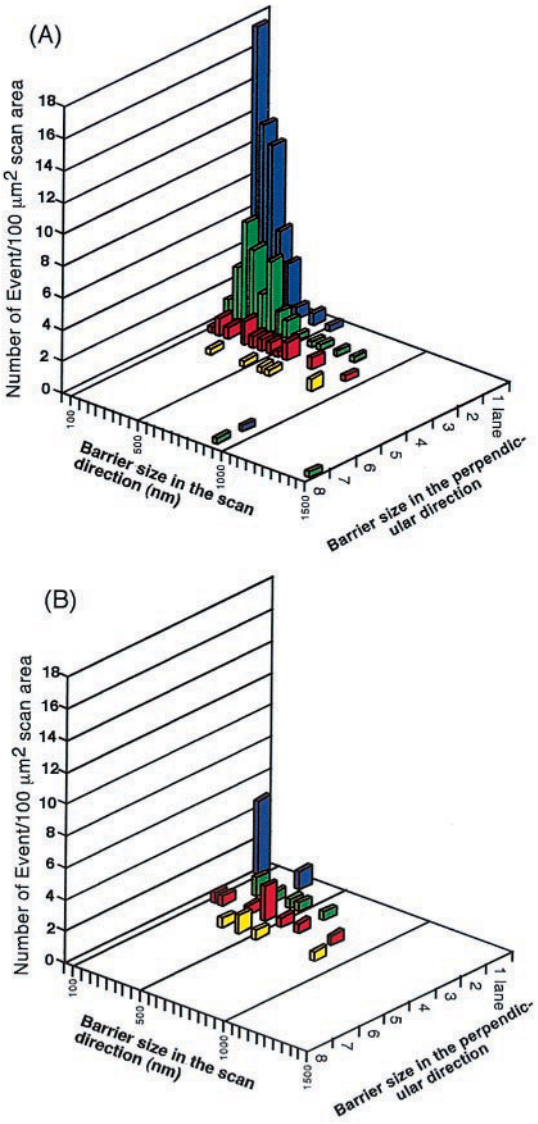

FIGURE 8 Histogram of the nonelastic barrier size. A scan was performed at 1.0 μm/s, using (*A*) a Qa-2 antibody-coated bead attached to the cell membrane (the total scan area was 269.1 μm^2) and (*B*) a bead that is not coated with antibody and, therefore, is not attached to the cell membrane, but contacts the membrane (the total scan area was 172.1 μm^2). The size was evaluated in terms of the scan direction and its perpendicular direction.

barriers for scanned beads, we scanned a bead that was not attached to the cell membrane but was held in contact with the membrane by the tweezers. Barriers in the range of 300–600 nm in the scan direction and from three to four lanes in the perpendicular direction were observed at the same frequency as with the attached antibody-coated beads (Fig. 8 *B*). We focused on the barriers smaller than 300 nm (Fig. 8 *A*) because those barriers were dependent upon the bound membrane components.

Because the scans were separated by 130 nm from each other (Fig. 1 *A*) and the contact length of the trapped

0.73-μm bead with the cell membrane was 220 nm (Fig. 6), there is about a 90-nm overlap region between the adjacent scans. A barrier in the overlap region should appear in the two adjacent scans if the barrier size is larger than the lateral distance between the membrane-bead linkages within the contact area. When the membrane-bead linkages are evenly distributed in the contact area, the probability that a barrier will encounter a dragged protein is higher in the area close to the centerline of the scan zone than in the peripheral areas. Although overlap might increase the size of the barriers, we did not find many instances where small barriers appeared in adjacent scans.

Domain size defined by SPT measurements of lateral diffusion of the GPI-anchored protein Thy-1 in fibroblast cells was 260–330 nm in diameter (Sheets et al., 1997). In this study, the barriers were normally not connected to form domains. There were 200–300-nm barriers that were frequently observed; however, the smallest barrier (50 nm $< d_s <$ 100 nm in scan direction, single lane in the perpendicular direction) was the most frequently observed. Barriers occupied less than 10% of the total scan area. The reasons for the confinement of GPI protein diffusion observed in the SPT studies are still controversial (Simson et al., 1998). In SPT, particles could be trapped by a flexible tether or in a viscous domain, whereas in SSR measurements we actively measure a membrane barrier at high resolution. The nature of the methodology might explain the difference between our estimation of barrier density and the one made by SPT.

CONCLUSION

This new SSR technology has allowed us to measure membrane viscous resistance and membrane barriers. Membrane viscous resistance to lateral transport scaled linearly with bead velocity and drastically increased with antibody density on the bead. The adjusted friction coefficient for 0.73-μm beads bound to the GPI-anchored membrane protein or Fl-PE was 1.13 pN/(μm/s) or 0.49 pN/(μm/s), respectively. The friction coefficient was inversely dependent upon temperature and decreased upon removal of extracellular carbohydrates. Membrane barriers consisted of elastic (cytoskeleton-dependent) and nonelastic barriers. The size of nonelastic barriers ranged from 50 nm to more than 1 μm. The technique exhibits several advantages compared with previous methods of single-particle tracking and one-dimensional scanning by laser tweezers: 1) two-dimensional scanning displayed barrier size and number; 2) elastic and nonelastic barriers can be distinguished; 3) continuous resistance can be observed, which allowed us to evaluate the membrane friction coefficient. With this technique, we have observed that cross-linking of GPI-linked protein recruits transmembrane proteins that encounter discontinuous and dynamic barriers.

APPENDIX: EFFECT OF TORQUE DURING A DRAG BY LASER TWEEZERS

When beads are dragged through the cell membrane with laser tweezers, a torque is generated on the bead. The force of the laser tweezers acts on the bead center while the friction force of the dragged membrane components acts on the bottom of the bead. Therefore, the torque could extract the cell membrane components from the membrane, followed by a bead rotation and reattachment to a cell component again. To determine the probability of extraction of the component in our experimental system, the force required to pull out the cell membrane component was estimated. Because the largest torque is applied to the edge of the contact area, we focused on the scale of the force at that point. If F_1 is the force on the bead center, F_v is the lateral viscous force on the cell membrane component, F_2 is the vertical force required to pull out the cell membrane component, d_1 is the radius of the bead, and d_2 is the radius of the contact area between the bead and the membrane (Fig. A1), the force in the direction of line a can be expressed by the equation

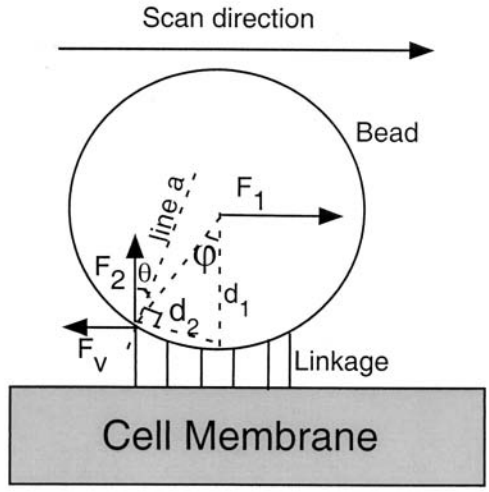

$$F_1 d_1 = F_2 d_2 \cos\theta - F_v \cos(90 - \theta) \quad (1)$$

Therefore,

$$F_2 = [F_1(d_1/d_2) + F_v \sin\theta]/\cos\theta \quad (2)$$

The diameter of the contact area between the 0.73-μm ($= 2d_1$) bead and the cell membrane is 0.22 μm ($= 2d_2$) because

$$\cos\varphi = \cos(2\theta) = 1 - d_2^2/(2d_1^2) \quad (3)$$

When a force of 4.3 pN ($= F_1$, the highest force in Fig. 4, stage speed = 2.9 μm/s) is applied to the bead in parallel with the cell membrane and the lateral viscous force by the cell membrane components at the edge ($= F_v$) is assumed to be 0.43 pN, the vertical force at the edge of the contact area ($= F_2$) is estimated to be 14.3 pN. Even if F_v is 4.3 pN, F_2 is estimated to be 15.1 pN, which is not so different from the above value. When the bead coated with the low concentration of Qa-2 antibody (Qa-2:fluorescein = 1:9) was attached to the edge of the cell membrane, 41% of Qa-2 molecules were extracted by laser tweezers with a maximum force of 24 pN (the velocity was less than 0.5 μm/s). Therefore, in the case of higher antibody concentration, we can anticipate that the probability of the extraction of the cell membrane component by 14.3–15.1 pN is much lower than 41%.

We thank Dr. Michael Edidin (Johns Hopkins University) for giving us Qa-2 antibody and HEPA-OVA cells. We also thank Dr. Dan P. Felsenfeld, Dr. Catherine Galbraith, other members of the Sheetz laboratory, and Dr. Ken Ritchie (ERATO, JST) for helpful discussions about this work. We thank Leslie Eibest for the operation of the scanning electron microscope and Dr. Jerry Norwich (University of California at San Diego) and Dr. Hie P. Ting Beal (Duke University) for their help with the SEM fixation protocol.

This work was supported by grants from the National Institutes of Health and the Muscular Dystrophy Association.

REFERENCES

Anderson, R. G. 1998. The caveolae membrane system. *Annu. Rev. Biochem.* 67:199–225.

Bussell, S. J., D. L. Koch, and D. A. Hammer. 1995a. Effect of hydrodynamic interaction on the diffusion of integral membrane proteins: tracer diffusion in organelle and reconstituted membranes. *Biophys. J.* 68: 1828–1835.

Bussell, S. J., D. L. Koch, and D. A. Hammer. 1995b. Effect of hydrodynamic interactions on the diffusion of integral membrane protein: diffusion in plasma membrane. *Biophys. J.* 68:1836–1849.

Dai, J., and M. P. Sheetz. 1995. Mechanical properties of neuronal growth cone membranes studied by tether formation with laser optical tweezers. *Biophys. J.* 68:988–996.

Dodd, T. L., D. A. Hammer, A. S. Sangani, and D. L. Koch. 1995. Numerical simulations of the effect of hydrodynamic interactions on diffusivities of integral membrane proteins. *J. Fluid Mech.* 293:147–180.

Edidin, M. 1997. Lipid microdomains in cell surface membranes. *Curr. Opin. Struct. Biol.* 7:528–532.

Edidin, M., S. C. Kuo, and M. P. Sheetz. 1991. Lateral movements of membrane glycoproteins restricted by dynamic cytoplasmic barriers. *Science.* 254:1379–1382.

Edidin, M., and I. Stroynowski. 1991. Differences between the lateral organization of conventional and inositol phospholipid-anchored membrane proteins. A further definition of micrometer scale membrane domains. *J. Cell. Biol.* 112:1143–1150.

Endere, T., T. Ha, D. F. Ogletree, D. S. Chemla, C. Magowan, and S. Weiss. 1997. Membrane specific mapping and colocalization of material and host skeletal proteins in the *Plasmodium falciparum* infected erythrocyte by dual-color near-field scanning optical microscopy. *Proc. Natl. Acad. Sci. USA.* 94:520–525.

Evans, E., D. Berk, and A. Leung. 1991. Detachment of agglutinin-bonded red blood cells. I. Forces to rupture molecular point attachments. *Biophys. J.* 59:838–848.

Felsenfeld, D. F., D. P. Choquet, and M. P. Sheetz. 1996. Ligand binding regulates the directed movement of $\beta 1$ integrins on fibroblasts. *Nature.* 383:438–440.

Gelles, J., B. J. Schnapp, and M. P. Sheetz. 1988. Tracking kinesin-driven movements with nanometre-scale precision. *Nature.* 331:450–453.

Hahn, A. B., H. Tian, G. Wiegand, and M. J. Soloski. 1992. Signals delivered via the Qa-2 molecule can synergize with limiting anti-CD3-induced signals to cause T lymphocyte activation. *Immunol. Invest.* 21:203–217.

Hwang, J., L. A. Gheber, L. Margolis, and M. Edidin. 1998. Domains in cell plasma membranes investigated by near-field scanning optical microscopy. *Biophys. J.* 74:2184–2190.

Kirchausen, T., J. S. Bonifacino, and H. Riezman. 1997. Linking cargo to vesicle formation+ receptor tail interactions with coat proteins. *Curr. Opin. Cell. Biol.* 9:488–495.

Koppel, D. E., M. P. Sheetz, and M. Schindler. 1981. Matrix control of protein diffusion in biological membranes. *Proc. Natl. Acad. Sci. USA.* 78:3576–3580.

Kucik, D. F., S. C. Kuo, E. L. Elson, and M. P. Sheetz. 1991. Preferential attachment of membrane glycoproteins to the cytoskeleton at the leading edge of lamella. *J. Cell. Biol.* 114:1029–1036.

Kucik, D. F., E. L. Elson, and M. P. Sheetz. 1999. Weak dependence of membrane protein aggregates on aggregate size supports a viscous model of retardation of diffusion. *Biophys. J.* 76:314–322.

Kusumi, A., and Y. Sako. 1996. Cell surface organization by the membrane skeleton. *Curr. Biol. Cell Biol.* 8:566–574.

Kusumi, A., Y. Sako, and M. Yamamoto. 1993. Confined lateral diffusion of membrane receptors as studied by single particle tracking (nanovid microscopy). *Biophys. J.* 65:2021–2040.

Lee, G. M., F. Zhang, A. Ishihara, C. L. McNeil, and K. A. Jacobson. 1993. Unconfined lateral diffusion and an estimate of pericellular matrix viscosity revealed by measuring the mobility of gold-tagged lipids. *J. Cell Biol.* 120:25–35.

McConville, M. J., and M. A. J. Ferguson. 1993. The structure, biosynthesis and function of glycosylated phosphatidylinositols in the parasitic protozoa and higher eukaryotes. *Biochem. J.* 294:305–324.

Saffman, P. G., and M. Delbruck. 1975. Brownian motion in biological membranes. *Proc. Natl. Acad. Sci. USA.* 72:3111–3113.

Sako, Y., and A. Kusumi. 1995. Barriers for lateral diffusion of transferrin receptor in the plasma membrane as characterized by receptor dragging by laser tweezers. *J. Cell. Biol.* 129:1559–1574.

Sako, Y., and A. Kusumi. 1998. Cytoplasmic regulation of the movement of E-cadherin on the free cell surface as studied by optical tweezers and single particle tracking: corralling and tethering by the membrane skeleton. *J. Cell Biol.* 140:1227–1240.

Saxton, M. J. 1990. Lateral diffusion in a mixture of mobile and immobile particles. A Monte Carlo study. *Biophys. J.* 58:1303–1306.

Schroder, O., W. Rathner, W. F. Caspary, and J. Stein. 1996. Bile acid-induced increase of rat colonic apical membrane fluidity and proton permeability. *Z. Gastroenterol.* 34:365–370.

Sheets, E. D., G. M. Lee, R. Simons, and K. A. Jacobson. 1997. Transient confinement of a glycosylphosphatidylinositol-anchored protein in the plasma membrane. *Biochemistry.* 36:12449–12458.

Sheetz, M. P., S. Turney, H. Qian, and E. L. Elson. 1989. Nanometre-level analysis demonstrates that lipid flow does not drive membrane glycoprotein movements. *Nature.* 340:284–288.

Shenoy-Scaria, A., J. Kwong, T. Fujita, M. W. Olszowy, A. S. Shaw, and D. M. Lublin. 1992. Signal transduction through decay-accelerating factor. *J. Immunol.* 149:3535–3541.

Simmons, R. M., J. T. Finer, S. Chu, and J. A. Spudich. 1996. Quantitative measurements of force and displacement using an optical trap. *Biophys. J.* 70:1813–1822.

Simons, K., and E. Ikonen. 1997. Sphingolipid-cholesterol rafts in membrane trafficking and signaling. *Nature.* 387:569–572.

Simson, R., B. Yang, S. E. Moore, P. Doherty, F. S. Walsh, and K. A. Jacobson. 1998. Structural mosaicism on the submicron scale in the plasma membrane. *Biophys. J.* 74:297–308.

Stefanova, I., V. Horejsi, I. J. Ansotegui, W. Knapp, and H. Stockinger. 1991. GPI-anchored cell-surface molecules complexed to protein tyrosine kinase. *Science.* 254:1016–1019.

Takeuchi, M., H. Miyamoto, Y. Sako, H. Komizu, and A. Kusumi. 1998. Structure of the erythrocyte membrane skeleton as observed by atomic force microscopy. *Biophys. J.* 74:2171–2183.

Tees, F. J., and H. L. Goldsmith. 1996. Kinetics and locus of failure of receptor-ligand-mediated adhesion between latex spheres. *Biophys. J.* 71:1102–1114.

Tomishige, M., Y. Sako, and A. Kusumi. 1998. Regulation mechanism of the lateral diffusion of band 3 in erythrocyte membranes by the membrane skeleton. *J. Cell Biol.* 142:989–1000.

Uchida, N., Y. Honjo, Johnson, K. R., Wheelock, and M. Takeichi. 1996. The catenin/cadherin adhesion system is localized in synaptic junctions bordering transmitter release zones. *J. Cell. Biol.* 135:767–779.

Zhao, D. L., and B. H. Hirst. 1990. Bile salt-induced increases in duodenal brush-border membrane proton permeability, fluidity and fragility. *Dig. Dis. Sci.* 35:589–595.